CHAPTER 2

Propellers

Chapter Outline

2.1. Introduction

Ships are predominantly equipped with 'simple' screw propellers. Special means of propulsion are covered towards the end of this chapter.

We will limit ourselves in the following to ships equipped with propellers. Propellers turning clockwise seen from aft are 'right-handed'. In twin-screw ships, the starboard propeller is usually right-handed and the port propeller left-handed. The propellers are then turning outwards. The propeller geometry is given in technical drawings following a special convention, or in thousands of offset points or spline surface descriptions, similar to the ship geometry. The complex propeller geometry is usually characterized by a few parameters. These include (Fig. 2.1):

- Propeller diameter D.
- Boss (or hub) diameter d.

Practical Ship Hydrodynamics. DOI: 10.1016/B978-0-08-097150-6.10002-8

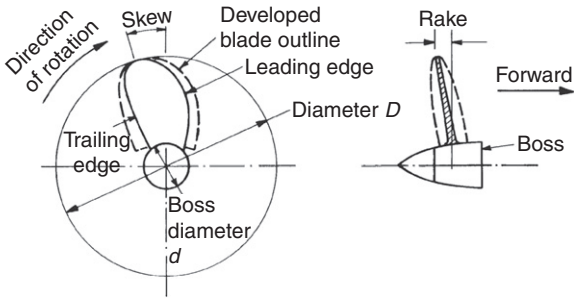

Figure 2.1:
Propeller geometry

- Propeller blade number Z.
- Propeller pitch P.

A propeller may be approximated by a part of a helicoidal surface which in rotation screws its way through the water. A helicoidal surface is generated as follows. Consider a line AB perpendicular to a line AA′ as shown in Fig. 2.2. AB rotates around the axis of AA′ with uniform angular velocity while moving along AA′ with uniform speed. AB then forms a helicoidal surface. Its pitch is the distance AA′. A propeller with a flat face and radially constant pitch would trace out a helicoidal surface. In reality, ship propellers often have neither a radially constant pitch nor a flat face. Then averaging in the circumferential direction creates a flat reference line to define the pitch as a function of the radius. Again averaging in a radial direction may define an average pitch P used to describe the propeller globally. Alternatively, the pitch at one radial position, typically $0.7R = 0.35D$, is taken as a single value to represent the radial pitch distribution.

- Disc area $A_0 = \pi D^2/4$.
- Projected area A_P.
- The blade area can be projected on to a plane normal to the shaft yielding the projected outline. Usually the area of the boss is not included.

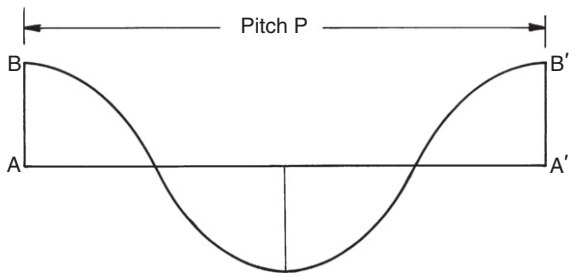

Figure 2.2:
Helicoidal surface defining pitch

- Expanded blade area A_E. The expanded outline is obtained if the circumferential chord of the blade is set out against the radius. The area of the formed outline is A_E.
- Skew (back). The line of the half chord length of each radial cross-section of the propeller is usually not a straight line, but curved back relative to the rotation of the blade. Skew is usually expressed as the circumferential displacement of the propeller tip made non-dimensional by the propeller diameter. Skew back evens out (to some extent) the influence of a highly non-uniform wake field and reduces peak values of propeller-induced vibrations. Modern ship propellers always have some skew back.
- Rake i_G. The face of the propeller may be tilted versus the normal plane on the propeller shaft. The tilt is usually backwards to increase the clearance between the blade tip and the hull.
- Profile shape. A propeller section at a given radius is the intersection between the blade and a circular cylinder of that radius. The section is then laid out flat (developed) and displayed as a two-dimensional profile. Historically, the early propeller designs had a flat face and circular cross-sections, which were then completely described by the blade width and maximum thickness. Today's profiles are far more complicated, but again usually characterized by a few parameters. The camber line is the line through the mid-thickness of the profile. If this line is curved, the profile is 'cambered'. The chord is the line joining the leading edge and the trailing edge. The camber is the maximum distance between the camber line and the chord. Profile sections are often defined by specifying the ordinates of the face and back as measured from the camber line.

Some of these data are often given as non-dimensional ratios:

- d/D;
- A_E/A_0;
- P/D;
- i_G.

The blade number Z is an important parameter for propeller-induced vibration. In general, odd numbers Z feature better vibration characteristics than even numbers. High blade numbers reduce vibration problems (due to less pronounced pressure peaks), but increase manufacturing costs. For large ships, blade numbers of four to seven are typical. For small boats, blade numbers of two to four are typical. The propellers for large ships are always tailored towards the specific ship and involve extensive hydrodynamic analyses. The propellers for boats are often mass-produced.

Typical extended blade area ratios are $0.3 < A_E/A_0 < 1.5$. Area ratios above 1 mean overlapping blades which are expensive to manufacture. A_E/A_0 is chosen such that the blade load is kept low enough to avoid unacceptable cavitation. Therefore A_E/A_0 increases with propeller load (thrust per propeller area A_0). The propeller efficiency decreases with A_E/A_0

since the increased area also increases frictional losses. Larger A_E/A_0 also often demands higher blade numbers to avoid too small side ratios for the blades.

2.2. Propeller Curves

Thrust T and torque Q are usually expressed as functions of rpm n in non-dimensional form as:

$$K_T = \frac{T}{\rho \cdot n^2 \cdot D^4} \tag{2.1}$$

$$K_Q = \frac{Q}{\rho \cdot n^2 \cdot D^5} \tag{2.2}$$

The force T is made non-dimensional by the propeller disk area times the stagnation pressure based on the circumferential speed, omitting a factor $\pi^2/8$. The moment Q is made non-dimensional by the additional length D, i.e. the propeller diameter.

The advance number J is defined as $J = V_A/(nD)$. V_A is the average inflow speed to the propeller. The propeller open-water efficiency is derived from thrust and torque coefficients and the advance number:

$$\eta_0 = \frac{T \cdot V_A}{2\pi \cdot n \cdot Q} = \frac{K_T \cdot \rho \cdot n^2 \cdot D^4}{K_Q \cdot \rho \cdot n^2 \cdot D^4} \cdot \frac{V_A}{2\pi \cdot n} = \frac{K_T}{K_Q} \cdot \frac{J}{2\pi} \tag{2.3}$$

K_T, K_Q, and η_0 are displayed over J. The curves are mainly used for propeller optimization and to determine the operation point (rpm, thrust, torque, power) of the ship. While the use of diagrams in education is still popular, in practice computer programs are almost exclusively used in propeller design. These represent traditionally the curves as polynomials in the form:

$$K_T = \sum C_T \cdot J^s \cdot \left(\frac{P}{D}\right)^t \cdot \left(\frac{A_E}{A_0}\right)^u \cdot Z^v \tag{2.4}$$

with tables of coefficients:

C_T	s	t	u	v
0.00880496	0	0	0	0
−0.20455403	1	0	0	0
…	…	…	…	…
−0.00146564	0	3	2	2

For standard Wageningen propellers the table consists of 49 coefficients for K_T and 56 coefficients for K_Q. While this may appear tedious, it is easy to program and fast to evaluate either by higher programming languages or spreadsheets. Diagrams are still popular in practice for documentation and visualization of tendencies.

Another important open-water parameter is the thrust loading coefficient:

$$C_{Th} = \frac{T}{\rho \cdot V_A^2 \cdot D^2 \cdot \frac{\pi}{8}} \tag{2.5}$$

This coefficient makes the thrust non-dimensional with the propeller disk area times stagnation pressure based on the propeller inflow velocity. Sometimes C_{Th} is also plotted explicitly in propeller characteristics diagrams, but sometimes it is omitted as it can be derived from the other quantities.

Figure 2.3 shows a typical propeller diagram. K_T and K_Q decrease monotonously with J. The efficiency η_0 has one maximum.

The open-water diagrams are based on stationary flow. They are only suitable for the case when the ship moves steadily ahead. For cases where the speed is changed, so-called four-quadrant diagrams are used. The name derives from a classification into four possible combinations:

- ship has forward speed, propeller delivers forward thrust;
- ship has forward speed, propeller delivers reverse thrust;
- ship has reverse speed, propeller delivers forward thrust;
- ship has reverse speed, propeller delivers reverse thrust.

The results of corresponding open-water tests are displayed in diagrams as shown in Fig. 2.4. The abscissa is the effective advance angle β defined by:

$$\tan \beta = \frac{V_A}{0.7 \cdot \pi \cdot n \cdot D} \tag{2.6}$$

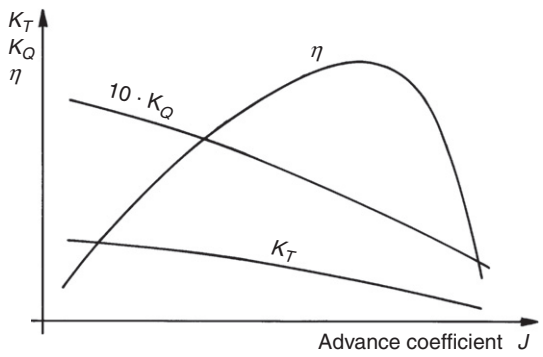

Figure 2.3:
Propeller diagram

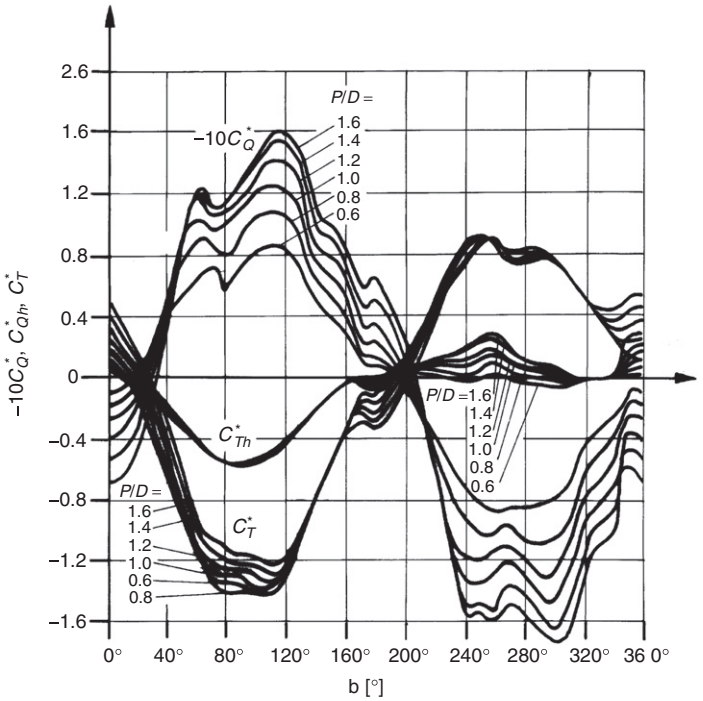

Figure 2.4:
Four-quadrant diagram for propellers

Displayed are non-dimensional modified thrust and torque coefficients:

$$C_{Th}^{*} = \frac{T}{\rho \cdot V_R^2 \pi D^2/8} \tag{2.7}$$

$$C_{Q}^{*} = \frac{Q}{\rho \cdot V_R^2 \pi D^3/8} \tag{2.8}$$

with $V_R = \sqrt{V_A^2 + (0.7\pi nD)^2}$.

Four-quadrant diagrams require considerably higher experimental effort than regular open-water diagrams. They are only available for some selected propellers. Four-quadrant diagrams are mainly used in computer simulations of ship maneuvers.

2.3. Analysis of Propeller Flows

2.3.1. Overview of Methods

Propellers create thrust as each of the blades is subject to local lift forces. Ideally, this lift is created with minimum drag losses. This basic goal is the same for other foil flows,

e.g. airfoils, ship rudders, etc. Each propeller section resembles a cross-section of a foil. However, ship propellers feature short and stubby blades with a much smaller span-to-chord ratio than in aeronautical foils. The reason is that the limited diameter and the danger of cavitation impose more severe restrictions on ship propellers.

The small span-to-chord ratio of a ship propeller blade is one of the reasons why ship propeller flows are so complex. All two-dimensional approaches to model the flow around a propeller blade (like lifting-line theories) introduce considerable errors that must be corrected afterwards. Lifting-line approaches are still popular in propeller design as a preliminary step, before more powerful, but also more expensive, three-dimensional methods are employed. Many lifting-line codes in use today can be traced back to a fundamental formulation given by Lerbs (1952, 1955).

The advent of high-skew propellers necessitated truly three-dimensional theories to model the flow around the propeller. Empirical corrections for the lifting-line method could no longer be applied satisfactorily to the new and more complex propeller geometries. The approach was then to use lifting-line methods for an initial design serving as a starting point for more sophisticated methods which could then serve to answer the following questions:

- Will the propeller deliver the design thrust at the design rpm?
- What will be the propeller (open-water) efficiency?
- How will the propeller perform at off-design conditions?
- Will the pressure distribution be such that the propeller features favorable cavitation characteristics?
- What are the time-dependent forces and moments from the propeller on the propeller shaft and ultimately the shaft bearings?
- What are the propeller-induced pressures at the ship hull (exciting vibrations and noise)?

These more sophisticated three-dimensional propeller theories used in practical propeller design today are lifting-surface methods, namely vortex-lattice methods, which do not consider the blade thickness, and boundary element methods or panel methods, which do consider the blade thickness. Field methods are increasingly employed for advanced propulsors, particularly for off-design conditions involving cavitation.

The main methods in increasing complexity are listed below with their respective advantages and disadvantages:

- *Momentum theory.* The propeller is reduced to an actuator disk which somehow creates a pressure jump in the flow. Thrust and corresponding delivered power are expressed by increased velocities in the propeller plane and the contracted wake downstream of this plane. This simple model is unsuitable for propeller design, but popular as a simple

propeller model in RANSE ship computations and useful in understanding some basic concepts of propeller flows.
  + Simple and fast; yields ideal efficiency η_i
  − Rotative and viscous losses not modeled; momentum theory is no method to design propellers or analyze given propeller designs
- *Lifting-line method.* Propeller blade is reduced to radially aligned straight vortices (lifting lines). The vortex strength varies over the radius. Free vortices are shed in the flow.
  + Proven in practice; suitable for initial design of propellers, rotative losses reflected in model; viscous losses incorporated by empirical corrections
  − Does not yield complete propeller geometry; cross-sections found, but angle of incidence and camber require corrections; no simple way to consider skew
- *Lifting-surface method, especially vortex-lattice method.* Propeller blade is reduced to a grid of horseshoe vortices; pressure distribution on the blade follows from Bernoulli's law from the induced velocities; pressure distribution yields forces and moments for the whole propeller.
  + Blade modeled three-dimensionally; corrections only necessary for viscous effects; good convergence to grid-independent solutions with grid refinement
  − More complex programming; pressure distribution must be corrected at the propeller hub
- *Boundary element method/panel method.* Exact formulation of the potential theory problem with source or dipole panels.
  + No simplifications besides the potential flow assumption; finite velocities in the hub region
  − Programming complex, especially for the Kutta condition; relatively large number of dipole and/or source panels necessary; flow near propeller tip still not well captured
- *RANSE method.* Field method formulation of the three-dimensional viscous flow.
  + Effective wake easily incorporated; viscous effects decreasing propeller efficiency directly captured; flow well captured also near hub and tip of propeller
  − Grid generation expensive; computation expensive; turbulence model questionable, possibly requiring LES.

Dedicated treatment of propeller flow analysis methods, predominantly based on lifting-surface and panel methods, can be found in, e.g., Breslin and Andersen (1994), Kinnas (1996), Streckwall (1993, 1999), and Carlton (2007).

2.3.2. Momentum Theory

Momentum theory models the propeller as a simple actuator disk accelerating the flow in the axial direction by somehow creating a pressure jump in the propeller plane. The propeller is then seen as a continuous circular disk with infinite blades and $A_E/A_0 = 1$. The

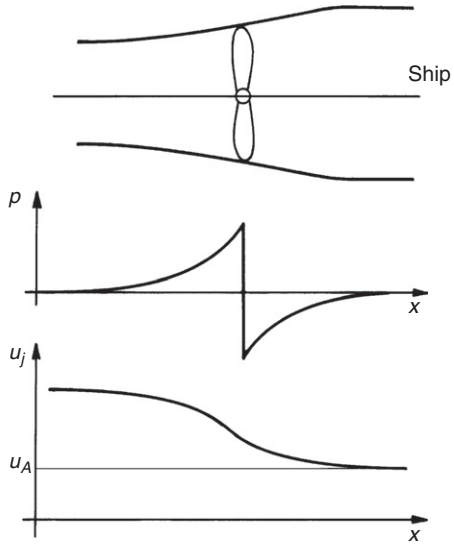

Figure 2.5:
Momentum theory considers propeller flow as one-dimensional flow with sudden pressure jump accelerating velocity from u_A to u_j

model is too crude to be of any value in propeller design, but allows some valuable insight into the global mechanisms of a propeller. The momentum theory regards inflow and outflow of the propeller plane as the flow through a tube of varying cross-section, but always of circular shape. Only the longitudinal velocity component is considered, i.e. the velocity is a scalar quantity.

The inflow to the propeller is given by $\rho \cdot u_A \cdot A_A$, where A_A is the cross-sectional area of the considered propeller plane. The propeller induces a velocity jump to the outflow velocity u_j and the cross-sectional area of the 'flow tube' is A_j. The thrust T is the change in the momentum:

$$T = \rho \cdot u_A \cdot A_A \cdot (u_j - u_A) \tag{2.9}$$

Continuity requires $A_j \cdot u_j = A_A \cdot u_A$, i.e. the flow contracts after the propeller due to the higher velocity (Fig. 2.5).

The velocity in the propeller plane is the average between the velocities far upstream and far downstream of the propeller in this model. Bernoulli's law couples the pressure to the velocity yielding qualitatively the distribution shown in Figure 2.5.

The actuator disk yields an ideal efficiency for the propeller of:

$$\eta_i = \frac{2u_A}{u_j + u_A} \tag{2.10}$$

This formula can be interpreted as follows. The smaller the increase in velocity due to the propeller, the better is the efficiency. If the velocity downstream is the same as the velocity upstream, the efficiency would be an ideal $\eta_i = 1$. (But no thrust would be produced.) The ideal efficiency can also be expressed in terms of the thrust loading coefficient C_{Th} as:

$$\eta_i = \frac{2}{1 + \sqrt{1 + C_{Th}}} \tag{2.11}$$

Thus a large thrust loading coefficient decreases the efficiency. The conclusion for practical propeller design is that usually the propeller diameter should be chosen as large as possible to increase the efficiency.

2.3.3. Lifting-Line Methods

Lifting-line methods still form a vital part of practical propeller design. They find the radial distribution of loading optimum with respect to efficiency as a first step to determine the corresponding blade geometry. Alternatively, the radial distribution of loading may be specified to determine the corresponding blade geometry (Lerbs 1952, 1955). Of course, this approach works only within limits. If unrealistic or too-demanding pressure distributions are specified, either no solution is found or the error in the framework of the theory is so large that the solution does not reflect reality.

Lifting-line methods for propellers were adapted from lifting-line theory for straight foils. We shall therefore briefly review the lifting-line theory for straight foils.

A straight line of vorticity creates lift orthogonal to the direction of the vortex line and the direction of the inflow (Fig. 2.6). Helmholtz's first and second laws state:

1. The strength of a vortex line is constant along its length.
2. A vortex line must be closed; it cannot end in the fluid.

As a consequence, the vortex lines on a foil are bent downstream at the end of the foil. Far downstream these vortex lines are closed again, but often 'far downstream' is interpreted as 'at infinity', i.e. the vortex line forms a semi-infinite horseshoe vortex. The vortex segment representing the foil is called the 'bound' vortex, as it always stays with the foil. The two vortex segments swept downstream are the 'trailing vortices', also denoted as axial vortices or tip vortices. The closing vortex segment far downstream is the 'starting' vortex.

In reality, the lift and thus the vorticity (vortex strength) are not constant over the foil span. This can be considered by approximating the continuous lift by a number of discrete, piecewise constant vortex segments. Each of these will then produce trailing vortices (Fig. 2.7). In sum, the vortex segments form a 'lifting line' of (stepwise) variable vorticity.

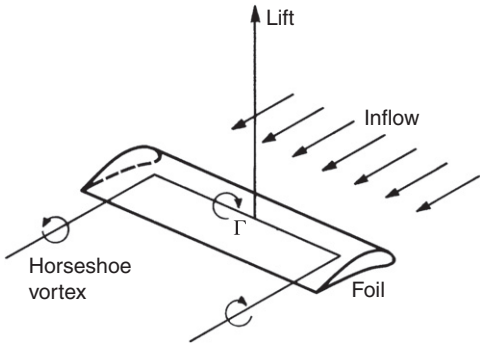

Figure 2.6:
Lifting-line theory is based on representing the foil by bound vortex and trailing vortices

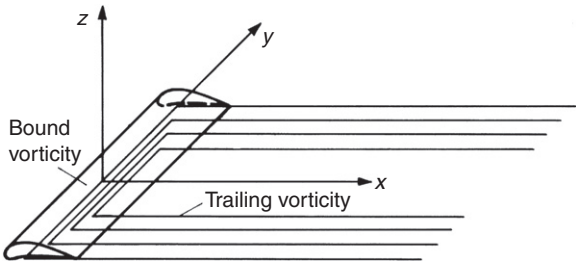

Figure 2.7:
A better model represents the foil by a distribution of horseshoe vortices

The trailing vortices induce a flow at the foil which is downward for positive lift. This velocity is therefore called downwash and changes the effective inflow angle experienced by each section of the foil.

The strengths of the individual vortex elements (each forming a closed or semi-infinite loop) are determined by requiring that there is no flow through the foil at a corresponding number of collocation points. This results in a system of linear equations which is solved numerically. Once all vortex strengths are known, the velocities and pressures can be evaluated everywhere. Lift and drag can then be computed.

For propellers, each blade is represented by one lifting line extending from hub to blade tip. Typically the lifting lines are straight with skew and rake being neglected at this point in the analysis. The proper end condition for the lifting line at the hub is unclear. Usually, the hub is neglected and the vorticity is required to go to zero as at the blade tip. This is called the 'hubless propeller assumption'. Lerbs argued that, near the hub, the blades are close enough together such that the positive pressure on the face of one blade is canceled by the negative pressure on the back of the adjacent blade. However, in practice

the lifting-line results near the hub, but also often near the blade, are unrealistic and are then manually corrected (smooth connection to the rest of the lift distribution based on human insight).

2.3.4. Lifting-Surface Methods

The discussion to substitute the lifting-line approach by lifting-surface theories dates back to the 1950s, but the realization of this goal was initially impossible for real ship propeller geometries due to insufficient computing power. The earliest lifting-surface attempts were based on mode functions which prescribed continuous distributions of surface singularities. At that time, the mode function approach was the ordinary procedure for solving lifting-line or two-dimensional wing section problems and naturally it was tried first. For lifting surfaces that had to fit propeller blades these mode functions needed a careful and complicated mathematical treatment. Their ability to describe arbitrary blade geometries was poor. The second generation of lifting-surface methods was developed around the late 1970s when sufficient computer power became widely available (Kerwin 1986). These methods used vortex lattices. Vortex-lattice methods are characterized by comparably simple mathematics. They can handle arbitrary blade geometries, but neither considers the true blade thickness, nor the propeller hub. This makes the theory of vortex-lattice methods more complicated than panel methods, but reduces the number of unknowns and thus the computational effort considerably. Despite the theoretical inferiority, vortex-lattice methods gave in benchmark tests of the ITTC for propellers with moderate skew-back results of comparable quality to panel methods. Figure 2.8 shows a typical discretization of the propeller blades and the wake. The hub is not modeled, which leads to completely unrealistic results in the immediate vicinity of the hub.

Vortex-lattice methods were extended in the 1990s to rather complicated propeller geometries, e.g. contra-rotating propellers, and unsteady propeller inflow (nominal wake computations). Cavitation may be simulated by additional singularities of both source and vortex type, but this remains a rather coarse approximation of the real phenomenon.

A complete vortex-lattice method (VLM) can be established on the basis of the lifting-line method just described. The lifting-line model was used to find a circulation Γ that corresponds to a given resultant flow direction at the lifting line and is able to provide the predetermined (design) thrust. With a vortex lattice instead of a lifting line, a model for the material blade is inserted. One can now really investigate whether a given geometry corresponds to a desired thrust, a task that is beyond the scope of a lifting-line theory.

Figure 2.9 shows a vortex-lattice system. The flow is generated by spanwise and (dependent) streamwise line vortices. Control points are positioned inside the loops of the vortex system. For steady flow, the vortex elements in the wake have the same strength in

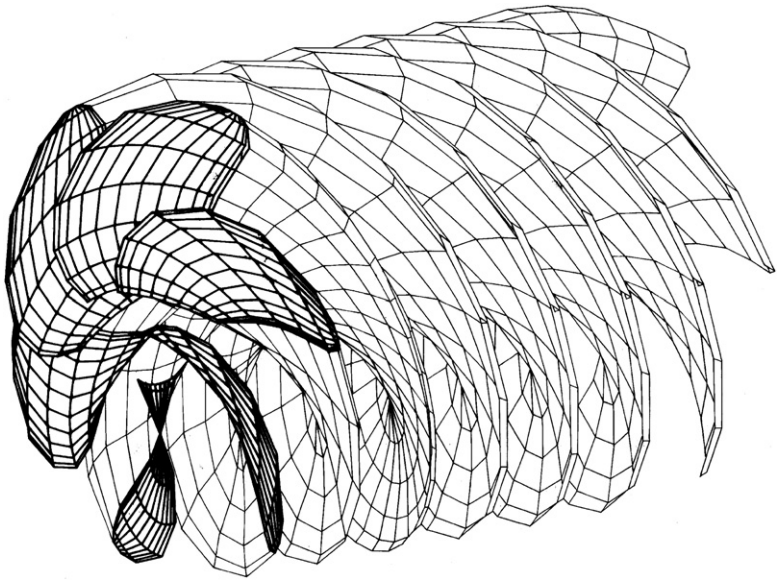

Figure 2.8:
Vortex-lattice model of a propeller and trailing wakes

each spanwise segment. The vertical vortex lines then cancel each other and a semi-infinite horseshoe vortex results. The most downstream control point is located at the trailing edge behind the last streamwise vortex, which is a very robust measure to enforce the Kutta condition.

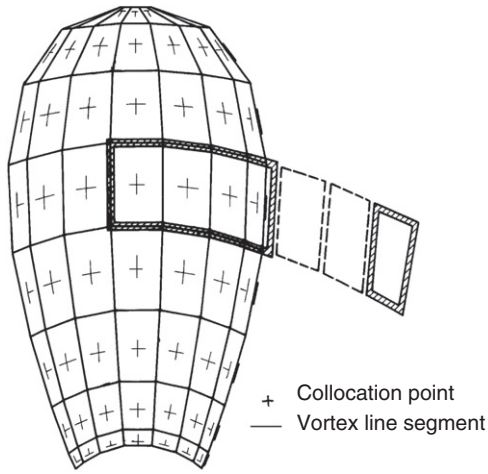

Figure 2.9:
Allocation of vortex-lattice elements on propeller blade

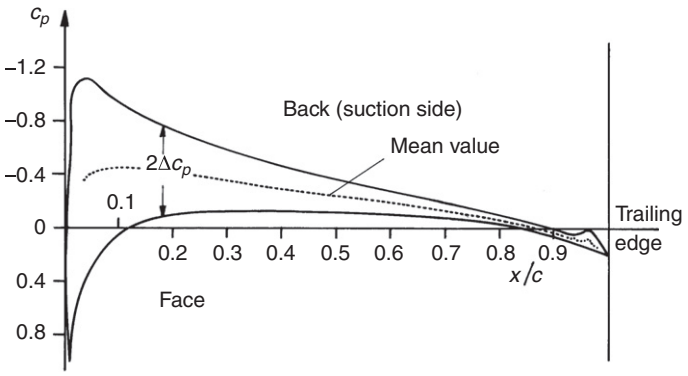

Figure 2.10:
Pressure distribution on a propeller blade profile

The kinematic boundary condition (zero normal velocity in a blade-fixed coordinate system), together with some basic relations between blade vortices and trailing vortices, is sufficient to calculate blade surface pressures and thus propeller thrust and torque. Although the kinematic condition is fulfilled on a zero-thickness blade, the influence of the blade thickness is not excluded. The thin-wing theory provides a simple formula to derive a source system from the slope of the section contours. This source system already enters the kinematic conditions and serves to correct the angle of attack of the blade sections for the displacement effect of the neighboring blades.

In most applications a 'frozen' vortex wake is used, i.e. the trailing vortex geometry is fixed from the start. A more or less empirical relation serves to prescribe the pitch of the helical lines. Since surface friction effects are not part of the solution, the forces and moments from the vortex lattice must be corrected subsequently. This is usually achieved by local section drag coefficients using empirical relations to express the Reynolds number dependence.

Figure 2.10 shows a typical pressure distribution for a propeller blade cross-section. The pressure coefficient can be decomposed into a mean value between both sides of the profile and a difference Δc_p. The pressure on the suction side is then obtained by subtracting Δc_p from the mean value, the pressure on the other side by adding Δc_p. Lifting-surface methods arrange the vortex and source elements on the mean chord surface of the blade. Following Bernoulli's law, the pressure can be computed from the velocities. This yields pressure distributions which usually reproduce the actual pressure distributions quite well except for a narrow region at the leading edge, which may extend to a length of approximately twice the nose radius. The sources yield the average pressure distribution and the vortex elements induce the pressure difference Δc_p. As the source strengths are explicitly derived from the change of the profile thickness in the longitudinal direction, the main problem is to determine the vortex strengths.

2.3.5. Boundary Element Methods

Panel methods were developed to overcome the disadvantage of an incomplete geometry model. Panel methods also model the blade thickness and include the hub in the numerical model. The development of panel methods for propellers was apparently not an easy task. After the ship hull flow could be treated by panel methods it took another decade until the late 1980s before the first successful panel approaches were established for propellers. The implementation of a robust Kutta condition is a decisive element of each propeller panel code, since it controls torque and thrust. In principle, there exist many possibilities to create panel codes, depending on panel type and the formulation of the problem (e.g. Kerwin et al. 1987). The following panel types are found:

- dipole panels;
- source panels;
- mix of dipole panels and source panels.

The problem may be formulated as:

- direct formulation (potential formulation); potential itself is the unknown;
- indirect formulation (velocity formulation); source or dipole strength is unknown.

For indirect formulations, Kerwin et al. (1987) show how a dipole-based formulation can be transformed to an equivalent vortex-based formulation.

The majority of the panel codes used for propellers follows Morino's approach (Morino and Kuo 1974, Morino 1975). Morino's approach is a direct formulation, i.e. it solves directly for the potential and determines velocities by numerical differentiation. The approach uses exclusively dipole panels, which discretize the surfaces of the propeller blades, the hub, and part of the wakes of each blade. The Kutta condition demands that at the trailing edge the pressure difference between face and back should vanish. This couples the dipoles on the wake to the dipoles on the propeller. The panels in the wake all have the same strength for steady flow conditions. The pitch of the wake is either specified by largely empirical relations or determined iteratively as part of the solution. The Kutta condition enforcing a vanishing pressure jump at the trailing edge is a non-linear condition requiring an iterative solution. The numerical implementation of the Kutta condition requires great care, since simplifications or conceptual errors in the physical model may strongly affect the computed lift forces.

The main problems of these methods lie in:

- numerical realization of the Kutta condition (stagnation point at the trailing edge);
- numerical (accurate) determination of velocity and pressure fields.

In the 1990s, panel methods were presented that were also capable of solving the problem for time-dependent inflow and ducted propellers (e.g. Kinnas 1996).

2.3.6. Field Methods

The common procedure to run unsteady propeller vortex-lattice or panel methods contains an inherent weakness. The ship is usually represented by the velocity field measured without the propeller at the propeller plane, i.e. the nominal wake. But in a real ship, the propeller rearranges the streamlines that reach the propeller plane, i.e. the propeller operates in the effective wake. There are measures to correct the nominal wake, but it is doubtful if these treat the details of the wake correctly.

No such complications arise in theory if viscous flow computations are employed. It is possible to interactively couple viscous flow computations for the ship based on RANSE solvers with potential flow computations for the propeller, e.g. vortex-lattice or panel methods. But increasingly the preferred option is to solve the flow around hull, propeller, and rudder using one RANSE model. The viscous flow representation for the propeller embedded in a viscous model for the ship makes all problems from decoupling ship flow and propeller flow vanish. By 2010, only selected analyses have appeared, but eventually this approach is expected to become standard for ship and propeller design.

Viscous flow computations are also able to deliver accurate flow details in the tip region of the propeller blade. Typical propeller geometries require careful grid generation to assure converged solutions. The warped propeller geometry makes grid generation particularly difficult, especially for high-skew propellers.

2.4. Cavitation

High velocities result in low pressures. If the pressure falls sufficiently low, cavities form and fill up with air coming out of solution and by vapor. This phenomenon is called cavitation. The cavities disappear when the pressure increases again. They grow and collapse extremely rapidly, especially if vapor is filling them. Cavitation involves highly complex physical processes with highly non-linear multi-phase flows which are subject to dedicated research by specialized physicists. We will cover the topic only to the extent that any naval architect should know. For a detailed treatment of cavitation for ship propellers, the reader is referred to the book by Isay (1989).

For ship propellers, the velocities around the profiles of the blade may be sufficiently high to decrease the local pressures to trigger cavitation. Due to the hydrostatic pressure, the total pressure will be higher on a blade at the 6 o'clock position than at the 12 o'clock position. Consequently, cavitating propellers will then have regions on a blade where alternately cavitation bubbles are formed (near the 12 o'clock position) and collapse again. The resulting rapid succession of explosions and implosions on each blade will have various negative effects:

- vibration;
- noise (especially important for navy ships like submarines);

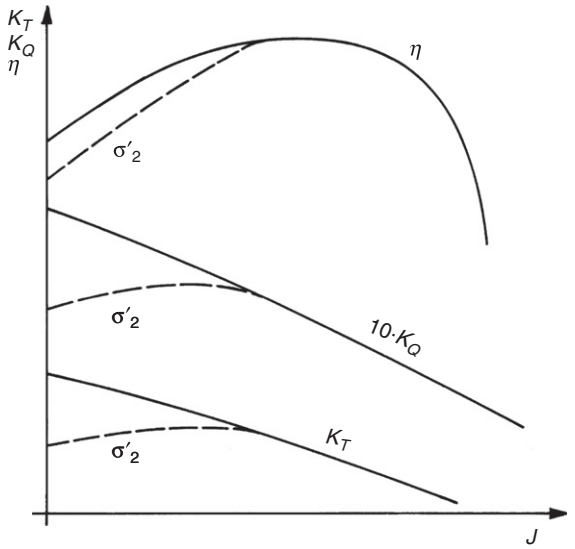

Figure 2.11:
Influence of cavitation on propeller characteristics

- material erosion at the blade surface (if the bubble collapse occurs there);
- thrust reduction (Fig. 2.11).

Cavitation occurs not only at propellers, but everywhere where locally high velocities appear, e.g. at rudders, shaft brackets, sonar domes, hydrofoils, etc.

Cavitation may be classified by:

- Location: tip cavitation, root cavitation, leading edge or trailing edge cavitation, suction side (back) cavitation, face cavitation, etc.
- Cavitation form: sheet cavitation, cloud cavitation, bubble cavitation, vortex cavitation.
- Dynamic properties of cavitation: stationary, instationary, migrating.

Since cavitation occurs in regions of low pressures, it is most likely to occur towards the blade tips where the local inflow velocity to the cross-sections is highest. But cavitation may also occur at the propeller roots near the hub, as the angle of incidence for the cross-sections is usually higher there than at the tip. The greatest pressure reduction at each cross-section profile usually occurs between the leading edge and mid-chord, so bubbles are likely to form there first.

In ideal water with no impurities and no dissolved air, cavitation will occur when the local pressure falls below vapor pressure. Vapor pressure depends on the temperature (Fig. 2.12). At 15°C it is 1700 Pa. In real water, cavitation occurs earlier, as cavitation nuclei like microscopic

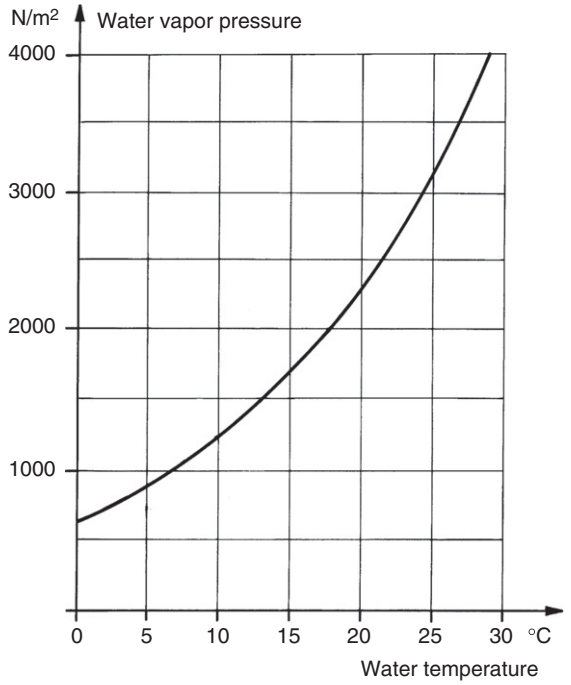

Figure 2.12:
Vapor pressure as a function of temperature

particles and dissolved gas facilitates cavitation inception. The cavitation number σ is a non-dimensional parameter to estimate the likelihood of cavitation in a flow:

$$\sigma = \frac{p_0 - p}{\frac{1}{2}\rho V_0^2} \tag{2.12}$$

p_0 is an ambient reference pressure and V_0 a corresponding reference speed. p is the local pressure. For $\sigma < \sigma_v$ (the cavitation number corresponding to vapor pressure p_v) the flow will be free of cavitation in an ideal fluid. In reality, one introduces a safety factor and sets a higher pressure than vapor pressure as the lower limit.

Cavitation is predominantly driven by the pressure field in the water. Cavitation avoidance consequently strives to control the absolute pressure minimum in a flow. This is achieved by distributing the thrust on a larger area, either by increasing the diameter or the blade area ratio A_E/A_0.

The most popular approach to estimate the danger of cavitation at a propeller uses Burill diagrams. These diagrams can only give a rough indication of cavitation danger. For well-designed, smooth propeller blades they indicate a lower limit for the projected area. Burill uses the coefficient τ_c:

$$\tau_c = \frac{T}{q_{0.7R}^2 A_p} \tag{2.13}$$

$$q_{0.7R} = \frac{1}{2}\rho V_R^2 \tag{2.14}$$

$$V_R = \sqrt{V_A^2 + (0.7\pi nD)^2} \tag{2.15}$$

V_R is the absolute value of the local velocity at 0.7 of the propeller radius. V_A is the inflow velocity to the propeller plane. A_p is the projected propeller area. Burill uses as reference pressure the atmospheric pressure plus the hydrostatic pressure at the propeller shaft:

$$p_0 = p_{atm} + \rho g h \tag{2.16}$$

The Burill diagram then yields limiting curves (almost straight) to avoid cavitation (Fig. 2.13). The curves have been transformed into algebraic expressions and are also included in propeller design programs. The upper limit for σ_c yields indirectly a minimum A_p which yields (for Wageningen B-series propellers) approximately the expanded blade area:

$$A_E \approx \frac{A_p}{1.067 - 0.229(P/D)} \tag{2.17}$$

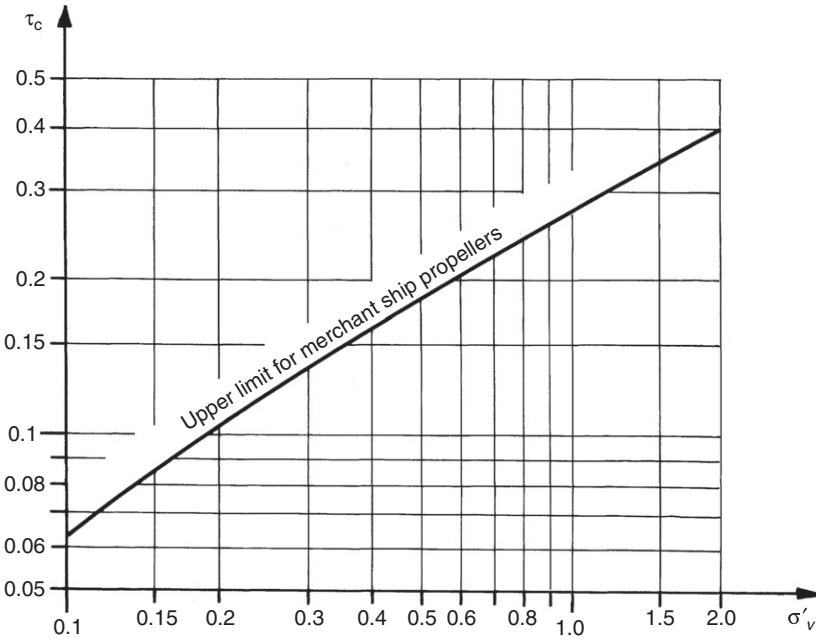

Figure 2.13:
Burill diagram

2.5. Experimental Approach

2.5.1. Cavitation Tunnels

Propeller tests (open-water tests, cavitation tests) are usually performed in cavitation tunnels. A cavitation tunnel is a closed channel in the vertical plane recirculating water by means of an impeller in the lower horizontal part. This way the high hydrostatic pressure ensures that even for reduced pressure in the tunnel, the impeller itself will not cavitate. The actual test section is in the upper horizontal part. The test section is provided with observation glass ports. The tunnels are designed to give (almost) uniform flow as inflow to the test section. If just the propeller is tested (with the driving shaft downstream), it is effectively tested in open water. Larger circulation tunnels also include ship models, thus testing the propeller in the ship wake. The ship models are sometimes shortened to obtain a thinner boundary layer in the aftbody (which thus resembles more the boundary layer in a large-scale model). Alternatively, sometimes grids are installed upstream to generate a flow similar to that of a full-scale ship wake. This requires considerable experience and is still at best a good guess at the actual wake field.

Vacuum pumps reduce the pressure in the tunnel and usually some devices are installed to reduce the amount of dissolved air and gas in the water. Wire screens may be installed to generate a desired amount of turbulence.

Cavitation tunnels are equipped with stroboscopic lights that illuminate the propeller intermittently such that propeller blades are always seen at the same position. The eye then perceives the propeller and cavitation patterns on each blade as stationary.

Usual cavitation tunnels have too much background noise to observe or measure the noise-making or hydro-acoustic properties of a propeller, which are of great interest for certain propellers, especially for submarines or antisubmarine combatants. Several dedicated hydro-acoustic tunnels have been built worldwide to allow acoustical measurements. The HYKAT (hydroacoustic cavitation tunnel) of HSVA is one of these.

2.5.2. Open-Water Tests

Although in reality the propeller operates in the highly non-uniform ship wake, a standard propeller test is performed in uniform flow yielding the so-called open-water characteristics, namely thrust, torque, and propeller efficiency.

The model scale λ for the model propeller should be the same as for the ship model in the propulsion tests. For many propulsion tests, the ship model scale is determined by the stock propeller, i.e. the closest propeller to the optimum propeller on stock at a model basin. The

similarity laws (see Section 1.2, Chapter 1) determine for geometrical and Froude similarity:

$$\left(\frac{V_A}{n\cdot D}\right)_s = \left(\frac{V_A}{n\cdot D}\right)_m \tag{2.18}$$

In other words, the advance number $J = V_A/(nD)$ is the same for model and full scale. J has thus a similar role for the propeller as the Froude number F_n has for the ship. V_A is the average inflow speed to the propeller, n the propeller rpm, and D the propeller diameter. $\pi\cdot n\cdot D$ is the speed of a point at the tip of a propeller blade in the circumferential direction.

The Reynolds number for a propeller is usually based on the chord length of one blade at 0.7 of the propeller radius and the absolute value of the local velocity V_R at this point. V_R is the absolute value of the vector sum of inflow velocity V_A and circumferential velocity:

$$V_R = \sqrt{V_A^2 + (0.7\pi nD)^2} \tag{2.19}$$

Propeller model tests are performed for geometrical and Froude similarity. It is not possible to keep Reynolds similarity at the same time. Therefore, as in ship model tests, corrections for viscous effects are necessary in scaling to full scale. ITTC 1978 recommends the following empirical corrections:

$$K_{Ts} = K_{Tm} - 0.3\cdot Z\cdot\left(\frac{c}{D}\right)_{r\,=\,0.7}\cdot\frac{P}{D}\cdot\Delta C_D \tag{2.20}$$

$$K_{Qs} = K_{Qm} + 0.25\cdot Z\cdot\left(\frac{c}{D}\right)_{r\,=\,0.7}\cdot\Delta C_D \tag{2.21}$$

c is the propeller blade chord length at $0.7R$, R the propeller radius, $\Delta C_D = C_{Dm} - C_{Ds}$ is a correction for the propeller resistance coefficient with:

$$C_{Dm} = 2\cdot\left(1 + 2\frac{t}{c}\right)\cdot\left(\frac{0.044}{R_n^{1/6}} - \frac{5}{R_n^{2/3}}\right) \tag{2.22}$$

$$C_{Ds} = 2\cdot\left(1 + 2\frac{t}{c}\right)\cdot\left(1.89 + 1.62\log\left(\frac{c}{k_p}\right)\right)^{-2.5} \tag{2.23}$$

Here t is the (maximum) propeller blade thickness and R_n is the Reynolds number based on V_R, both taken at $0.7R$. k_p is the propeller surface roughness, taken as $3\cdot 10^{-5}$ if not known otherwise.

2.5.3. Cavitation Tests

Cavitation tests investigate the cavitation properties of propellers. Experiments usually observe the following similarity laws:

- Geometrical similarity, making the propeller as large as possible while still avoiding tunnel wall effects.

- Kinematical similarity, i.e. the same advance number in model and ship, $J_m = J_s$.
- Dynamical similarity would require that model and full-scale ship have the same Froude and Reynolds numbers. Reynolds similarity is difficult to achieve, but the water speed is chosen as high as possible to keep the Reynolds number high and reduce scaling effects for the friction on the blades. Gravity effects are negligible in propeller flows, i.e. waves usually play no role. Thus the Froude number may be varied.
- Cavitation similarity requires the same cavitation numbers in model and full-scale ships. The tunnel pressure is adjusted to give the same cavitation number at the propeller shaft axis to approximate this condition.
- For similarity in bubble formation in cavitation, the Weber number should also be the same in model and full scale:

$$\left(\frac{\rho \cdot V_A^2 \cdot D}{T_e}\right)_m = \left(\frac{\rho \cdot V_A^2 \cdot D}{T_e}\right)_s \tag{2.24}$$

  where T_e is the surface tension and D the propeller diameter. This similarity law is usually violated.

The cavitation tests are performed for given inflow velocity and cavitation number, varying the rpm until cavitation on the face and back of the propeller is observed. This gives limiting curves $\sigma = \sigma(J)$ for cavitation-free operation. The tests are often performed well beyond the first inception of cavitation and then the extent and type of cavitation is observed, as often designers are resigned to accept some cavitation, but individual limits of accepted cavitation differ and are often subject to debate between shipowners, ship designers, and hydrodynamic consultants. The tests are usually based entirely on visual observation, but techniques have been developed to automatically detect and visualize cavitation patterns from video recordings. These techniques substitute the older practice of visual observation and manual drawings, making measurements by various persons at various times more objectively comparable.

2.6. Propeller Design Procedure

Traditionally, propeller design was based on design charts. These charts were created by fitting theoretical models to data derived from actual model or full-size tests and therefore their number was limited. By and large, propeller design was performed manually. In contrast, contemporary propeller design relies heavily on computer tools. Some of the traditional propeller diagrams, such as for the Wageningen B-series of propellers, have been transformed into polynomial expressions allowing easy interpolation and optimization within the traditional propeller geometries. This is still a popular starting point for modern propeller design. Then,

a succession of ever more sophisticated analysis programs is employed to modify and fine-tune the propeller geometry.

Propeller design is an iterative process to optimize the efficiency of a propeller subject to more or less restrictive constraints concerning cavitation, geometry, strength, etc. The severity of the constraints depends on the ship type. For example, submarine propellers have strict constraints concerning cavitation-induced noise. Subsequently the efficiencies of these propellers are lower than for cargo ships, but the primary optimization goal is still efficiency. A formal optimization is virtually impossible for modern propellers if the description of the geometry is based on (some hundreds of) offsets, as the evaluation of the efficiency based on CFD requires considerable time. Thus, while the word 'optimization' is often used, the final design is rather 'satisficing', i.e. a good solution satisfying the given constraints. However, parametric description coupled with efficient CFD and optimization schemes had allowed formal propeller optimization in industry by 2010.

Additional constraints are inherently involved in the design process, but often not explicitly formulated. These additional constraints reflect the personal 'design philosophy' of a designer or company and may lead to considerably different 'optimal' propellers for the same customer requirements. An example of such a 'design philosophy' could be the constraint that no cavitation should occur on the pressure side of the propeller. The following procedure will reflect the design philosophy of HSVA as detailed in Reich et al. (1997). The overall procedure will, however, be similar to any other state-of-the-art propeller design process. The main engine influences the propeller design primarily through the propeller rpm and delivered power. Modern turbo-charged diesels, almost exclusively used for cargo ships today, are imposing a rather narrow bandwidth for the operating point (rpm/power combination) of the propeller. We therefore limit ourselves to such cases where the rpm, the ship's speed, and an estimated delivered power P_D are specified by requirement. This covers more than 90% of the cases in practice.

The procedure follows a few main steps which involve model tests, analytical tools of successive sophistication and power, and some experience in deciding trade-offs in conflict situations:

1. Preparation of model
   Known at this stage:
   - experiments
   - rpm of the full-scale propeller n_s
   - ship speed V_s
   - estimate of delivered power for the ship P_D
   - ship hull form (lines plan)
   - classification society
   - often: number of blades Z
   - often: diameter of propeller D

Generally, the customer specifies within small margins what power P_D has to be delivered at what speed V_s and what is the rpm of the (selected) main engine. While in theory such a combination may be impossible to realize, in practice the shipyard engineers (i.e. the customers) have sufficient experience to estimate a realistic power for a shipowner-specified speed and rpm. The shipyard or another department in the model basin will specify a first proposal for the ship lines. Often, the customer will also already determine the number of blades for the propeller. A few simple rules gained from experience will guide this selection, e.g. if the engine has an even number of cylinders, the propeller should have an odd number of blades. The propeller of optimal efficiency can then be determined automatically based on the Wageningen B-series by computer codes. The performance of these older propellers is insufficient for today's expectations and the propeller thus determined will only be used as a starting point for the actual design. This procedure yields the average (or representative) pitch-to-diameter ratio P_m/D and the diameter D. An upper limit for the diameter is specified from the ship geometry. Sometimes the customer already specifies the diameter, otherwise it is a result of the optimization. The expanded area ratio A_E/A_0 is usually part of the optimization result, but may be restricted with respect to cavitation if problems are foreseen. In this case, a limiting value for A_E/A_0 is derived from Burill diagrams.

Then, from a database of stock propellers, the most suitable propeller is selected. This is the propeller with the same number of blades, closest in P_m/D to the optimized propeller. If several stock propellers coincide with the desired P_m/D, the propeller closest in A_E/A_0 among these is selected. A selection constraint comes from upper and lower limits for the diameter of the stock propeller which are based on experience for the experimental facilities. For example, for HSVA, the ship models may not exceed 11 meters in length to avoid the influence of canal restrictions, but should be larger than 4 meters to avoid problems with laminar flow effects. As the ship length is specified and the model scale for propeller and ship must be the same, this yields one of the constraints for upper and lower values of the diameter of the stock propeller. Usually, the search of the database is limited to the last 300 stock propellers, i.e. the most recent designs.

The selected stock propeller then determines the model scale and the ship model may be produced and tested. The output of the model tests relevant for the propeller designer is:

- nominal wake distribution (axial, tangential, and radial velocities in the propeller plane)
- thrust deduction fraction t
- effective wake fraction w
- relative rotative efficiency η_R
- delivered power P_D.

The delivered power P_D is of secondary importance (assuming that it is close to the customer's estimate). It indicates how much the later propeller design has to strive for a high efficiency. If the predicted P_D is considerably too high, then the ship form has to be changed and the tests repeated.

2. Estimate effective wake distribution full scale
   Known at this stage: all of the above and …
   number of blades Z
   diameter of propeller D
   blade area ratio A_E/A_0
   thrust deduction fraction t
   effective wake fraction w
   relative rotative efficiency η_R
   nominal wake field (axial, tangential, radial velocity components)

   Ship−propeller interaction is difficult to capture. The inflow is taken from experiments and based on experience modified to account for scale effects (model/full-scale ship). The radial distribution of the axial velocity component is transformed from the nominal (without propeller action) value for the model to an effective (with propeller) value for the full-scale ship. The other velocity components are assumed not to be affected. Several methods have been proposed to perform this transformation. To some extent, the selection of the 'appropriate' method follows rational criteria, e.g. one method is based on empirical data for full ships such as tankers, another method for slender ships such as container ships. But still the designer expert usually runs several codes, looks at the results and selects the 'most plausible' based on 'intuition'. The remaining interaction effects such as thrust deduction fraction t and relative rotative efficiency η_R are usually taken as constant with respect to the results of ship model tests with propellers.
3. Determine profile thickness according to classification society
   Known at this stage: all of the above
   Classification societies have simple rules to determine the minimum thickness of the foils. The rules of all major classification societies are implemented in programs that adjust automatically the (maximum) thickness of all profiles to the limit value prescribed by the classification society.
4. Lifting-line and lifting-surface calculations
   Known at this stage: all of the above and . . .
   max. thickness at few radii

   As additional input, default values are taken for profile form (NACA series), distribution of chord length and skew. If this step is repeated at a later stage, the designer may deviate from the defaults. At this stage, the first analytical methods are employed. A lifting-line method computes the flow for a two-dimensional profile, i.e. the three-dimensional flow is approximated by a succession of two-dimensional flows. This is numerically stable and effective. The method needs an initial starting value for the circulation distribution. This is taken as a semi-elliptic distribution. The computation then yields the optimal radial distribution of the circulation. These results are directly used for a three-dimensional

lifting-surface program. The lifting-surface code yields as output the radial distribution of profile camber and pitch.

5. Smoothing results of Step 4
   Known at this stage: all of the above and . . .
   radial distribution of profile camber (estimate)
   radial distribution of pitch (estimate)
   The results of the three-dimensional panel code are generally not smooth and feature singularities at the hub and tip of the propeller. The human designer deletes 'stray' points (point-to-point oscillations) and specifies values at hub and tip based on experience.
6. Final hydrodynamic analysis
   Known at this stage: all of the above (updated)
   The propeller is analyzed in all operating conditions using a lifting-surface analysis program and taking into account the complete wake distribution. The output can be broadly described as the cavitational and vibrational characteristics of the propeller. The work sometimes involves the inspection of plots by the designer. Other checks are already automated. Based on his 'experience' (sometimes resembling a trial-and-error process), the designer modifies the geometry (foil length, skew, camber, pitch, profile form and even, as a last resort, diameter). However, the previous steps are not repeated and this step can be treated as a self-contained module.
7. Check against classification society rules
   Known at this stage: all of the above (updated)
   A finite-element analysis is used to calculate the strength of the propeller under the pressure loading. The von Mises stress criterion is plotted and inspected. As the analysis is still limited to a radially averaged inflow, a safety margin is added to account for the real inflow. In most cases, there is no problem. But if the stress is too high in some region (usually the trailing edge), the geometry is adjusted and Step 6 is repeated. The possible geometry modifications at this stage are minor and local; they have no strong influence on the hydrodynamics and therefore one or two iterations usually suffice to satisfy the strength requirements.

2.7. Propeller-Induced Pressures

Due to the finite number of blades the pressure field of the propeller is unsteady if taken at a fixed point on the hull. The associated forces induce vibrations and noise. An upper limit for the maximum pressure amplitude that arises on the stern (usually directly above the propeller) is often part of the contract between shipyard and owner.

For many classes of ships the dominant source for unsteady hull pressures is the cavitation on the propeller blades. The effect of cavitation in computations of propeller-induced pressures is

usually modeled by a stationary point source positioned in the propeller plane. To assure similarity with the propeller cavitation, the source must be given an appropriate volume amplitude, a frequency of oscillation, and a suitable position in the propeller plane specified by a radius and an angle. As the propeller frequency is rather high, the dominant term in the Bernoulli equation is the time-derivative term. If mainly fluctuating forces from propeller-induced hull pressures are of interest, the pressure is therefore usually sufficiently well approximated by the term $-\rho\phi_t$, where ϕ denotes the potential on the hull due to the perturbations from the propeller.

If pressures and forces induced by a fluctuating source on solid boundaries are to be considered, the point source may be positioned underneath a flat plate to arrive at the simplest problem of that kind. The kinematic boundary condition on the plate is ensured via an image source of the same sign at the opposite side of the plate. For the pressure field on a real ship, this model is too coarse, as a real ship aftbody does not look like a flat plate and the influence of the free surface is neglected. Potential theory is still sufficient to solve the problem of a source near a hull of arbitrary shape with the free surface present. A panel method (BEM) easily represents the hull, but the free surface requires special treatment. The high frequency of propeller rpm again allows a simplification of the treatment of the free surface. It is sufficient to specify then at the free surface $z = \zeta$:

$$\phi(x, y, z = \zeta, t) = 0 \tag{2.25}$$

If the free surface is considered plane ($\zeta = 0$), $\phi = 0$ can be achieved by creating a hull image above the free surface and changing the sign for the singularities on the image panels. An image for the source that represents the cavity (again of opposite sign in strength) has to be introduced as well. The free surface can be considered in good approximation as a plane for low Froude numbers, such as typically encountered for tankers and bulkers, but it is questionable for moderate and high Froude numbers. A pronounced stern wave will have a significant effect on the wetted areas at the stern.

The main problem of the above procedure is the reliability of calculated cavity volumes.

2.8. Unconventional Propellers

Special means of propulsion are covered in greater detail in Schneekluth and Bertram (1998) and Carlton (2007). Unconventional propulsors have developed in various forms, for various special applications:

- Nozzled propellers. The (Kort) nozzle is a fixed annular forward-extending duct around the propeller. The propeller operates with a small gap between blade tips and nozzle internal wall, roughly at the narrowest point. The nozzle ring has a cross-section shaped as

a hydrofoil or similar section. Nozzled propellers have the following advantages and disadvantages:

+ At high thrust-loading coefficients, better efficiency is obtainable. For tugs and pusher boats, efficiency improvements of around 20% are frequently achievable. Bollard pull can be raised by more than 30%.
+ The reduction of propeller efficiency in a seaway is lower for nozzle propellers than for non-ducted propellers.
+ Course stability is substantially improved by the nozzle.
− Course-changing ability during astern operation is somewhat impaired.
− Owing to circulation in shallow water, the nozzle propeller tends to draw into itself shingle and stones. Also possible is damage due to operation in ice. This explains the rare application on seagoing ships.
− Due to the pressure drop in the nozzle, cavitation occurs earlier.

Nozzled propellers have been fitted frequently on tugs, fishing vessels, and inland water vessels.

- Contra-rotating propellers (CRP). Rotational exit losses amount to about 8−10% in typical cargo ships. Coaxial contra-rotating propellers (Fig. 3.15) can partially compensate these losses, increasing efficiency by up to 6% (Isay 1964). To avoid problems with cavitation, the after-propeller should have smaller diameter than the forward propeller. Contra-rotating propellers have the following advantages and disadvantages:
  + The propeller-induced heeling moment is compensated (this is negligible for larger ships).
  + More power can be transmitted for a given propeller radius.
  + The propeller efficiency is usually increased.
  − The mechanical installation of coaxial contra-rotating shafts is complicated, expensive and requires more maintenance.
  − The hydrodynamic gains are partially compensated by mechanical losses in shafting.

  Contra-rotating propellers are used on torpedoes due to the natural torque compensation. They are also found in some motorboats. For normal ships, the task of boring out the outer shafts and the problems of mounting the inner shaft bearings were not considered to be justified by the increase in efficiency (in times of relatively cheap fuel), although in the early 1990s some large tankers were equipped with contra-rotating propellers. The CRPs should not be confused with the Grim wheel, where the 'aft' propeller is not driven by a shaft. Unlike a CRP, the Grim wheel turns in the same direction as the propeller.
- Controllable-pitch propeller (CPP). CPPs with three to five blades are often used in practice and feature the following advantages and disadvantages:
  + Fast stop maneuvers are possible.
  + The main engine does not need to be reversible.
  + The CPP allows one to drive the main generator with the main engine which is efficient and cheap. Thus the electricity can be generated with the efficiency of the main engine

and using heavy fuel. Different ship speeds can be driven with constant propeller rpm as required by the generator.
  − Fuel consumption is higher. The higher propeller rpm at lower speed is hydrodynamically suboptimal. The CPP requires a bigger hub (0.3−0.32D). The pitch distribution is suboptimal. The usual radial direction, almost constant, pitch would cause negative angles of attack at the outer radii for reduced pitch, thus slowing the ship down. Therefore CPPs usually have higher pitch at the outer radii and lower pitch in the inner radii. The higher pitch in the outer radii necessitates also a larger propeller clearance.
  − Higher costs for propeller.

- Azimuthing propellers. Azimuthing propellers (a.k.a. rudder propellers, slewable propellers), usually equipped with nozzles, are not just a derivative of the well-known outboarders for small boats. Outboarders can only slew the propeller by a limited angle to both sides, while azimuthing propellers can cover the full 360°. Turning the propeller by 180° allows reversing the thrust. This astern operation is much more efficient than for conventional propellers turning in the reverse direction. By 2003, rudder propellers were available for up to 4000 kW permanent power. Podded drives housing an electric motor in the pod which drives the propeller(s) can be seen as a special case of azimuthing propellers.
- Podded drives. Podded drives are characterized by two main features: there is an electric motor inside a pod and the total unit is azimuthing. In 1990, the auxiliary vessel 'Seiti' was the first ship to be equipped with a pod drive. Within only a decade, pod drives became the dominant choice of propulsion for certain ship types. The hydrodynamic unit efficiency of pod drives is approximately 5% lower than that of an identical conventional propeller with a rudder as a unit. In many cases, in addition, some efficiency is lost for pod units, because the pod propeller cannot have optimal diameter due to the torque limitation of the pod motor. A small gain in propeller efficiency can be expected for twin pod arrangements because the inflow to the propeller is more uniform (absence of shafts and shaft brackets). This leads to better design conditions for the propeller and therefore to higher propeller efficiencies.

  Mewis (2001) gives advantages and disadvantages of pod drives:
  + More cargo space because the engine can be located more freely
  + Better maneuverability
  + Lower noise level
  + Low speeds are possible
  + Suited as booster drive in order to increase the speed
  + Less work expense in ship manufacturing
  + (Potentially) lower power requirement for twin screw ships
  − Higher capital costs
  − Diesel electric system required (power loss)
  − Increased power requirement for single screw arrangements

− Limitation in power (up to 32 MW in 2003)
− Limitation in speed (up to 30 knots in 2003).

The following order of suitability depending on ship type is given:

Very well suited: cruise liner, RoPax ferry, icebreaker
Well suited: supply vessel, bulker, tanker (single and twin screw)
Hardly suited: container vessel (single screw) $<$ 3000 TEU
Not well suited: container vessel (twin screw)
Not feasible: container vessel (single screw) $>$ 3000 TEU.

- Waterjets. Waterjets as alternative propulsive systems for fast ships, or ships operating in extremely shallow water, are discussed by, e.g., Allison (1993), Kruppa (1994), and Terswiga (1996). For high ship speed, restricted propulsor diameters and cavitation-free operation, conventional propellers reach their limits. Since these problems are not generally new, pumps were introduced as a propulsion system already in the early 1920s. These ancient pump systems already included in principle the same components as a modern waterjet: water inlets with inboard tubing system, the pump inducing energy to the water and finally the nozzle, which deals with the propulsive power. With the early waterjet systems, the steering of the vessel was performed separately by conventional rudders, whereas in modern systems the steering and reversing systems are integrated in the jets.

  Special attention has to be paid to the shape of the waterjet inlets to avoid excessive additional resistance, cavitation, and noise and on the other hand to ensure sufficient flow of the pump.

  Waterjet propulsion has become a popular propulsor choice for fast ships. The Royal Institution of Naval Architects has in addition hosted dedicated conferences on waterjet propulsion in 1994 and 1998 and the ITTC has a subcommittee reviewing the continuing progress on waterjets.

  The application of waterjets ranges from fast monohull car/passenger ferries to catamarans, motor yachts, speed boats, hydrofoils, and surface effect ships. Waterjets feature the following advantages and disadvantages:

  + Higher efficiency at speeds above 35 knots ($\eta > 0.8$)
  + No appendage resistance for shafts, brackets, rudders
  + Operability in shallow water
  + More flexibility in locating main engines
  + Much smaller risk of cavitation
  + Excellent maneuvering
  + More thrust with smaller impeller diameter
  + Lower noise development (-7 to -10 dB (A9))
  + No need for reversing gear (except when gas turbines are used as prime mover)
  − Drastically lower efficiency at lower speeds
  − Larger weight of the waterjet unit incl. the added water mass within the pump

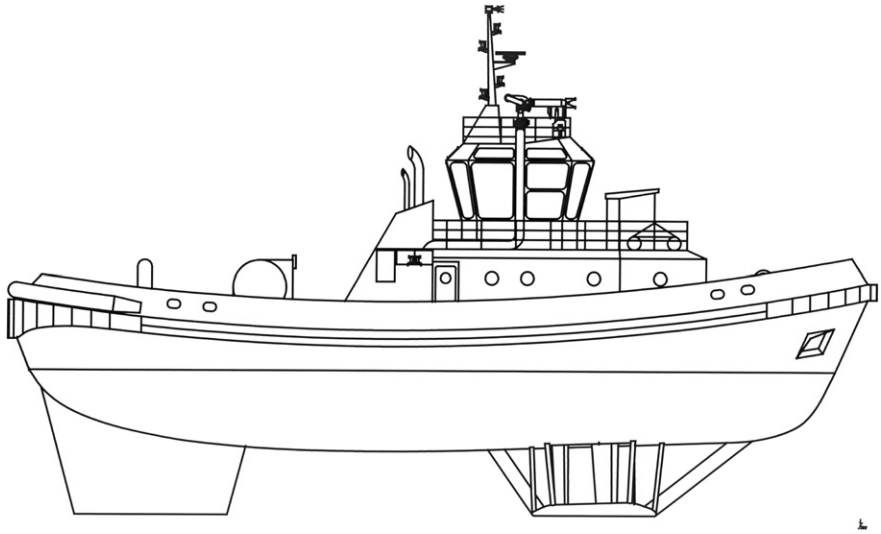

Figure 2.14:
Voith–Schneider propeller installed in a Voith water tractor tug. *Source: Voith Turbo*

– Power required to lift water from inlet to the nozzle level, especially for nozzle above water line (hydrofoils)
– Higher cost for pumps and inlets
– Larger space requirements inside hull.

Model tests with waterjets are mostly performed at high model speeds and therefore the available measuring time becomes relatively short so that the exact self-propulsion point is difficult to match. Therefore it is common practice that different runs will be performed for each speed with various impeller rpms. This procedure delivers a series of cross curves from which the actual self-propulsion point can be found at the condition that the residuary force is equal to the corresponding friction deduction.

- Surface-piercing propellers. Surface-piercing propellers operate only partially submerged, typically with 30–50% of the propeller being surfaced. The propeller blades are designed to operate such that the pressure face of the blade remains fully wetted and the suction side is fully ventilated or dry. Surface-piercing propellers are used on fast craft, typically racing boats and some fast naval vessels.
- Voith–Schneider propellers (cycloidal propellers). The Voith–Schneider propeller (VSP) is a cycloidal drive that combines propulsion and maneuvering. The VSP consists of a circular plate with an array of typically five vertical, foil-shaped blades. The plate is attached to the bottom of the vessel (Fig. 2.14). It rotates around a vertical axis. Each blade in turn can rotate around a vertical axis. An internal gear changes the angle of attack of the blades in sync with the rotation of the plate, so that each blade can provide thrust in the same direction. The VSP

makes vessels highly maneuverable, as the thrust can be adjusted in magnitude and direction arbitrarily without changing the engine's rpm, almost instantaneously. VSPs are usually arranged in tandem. It is widely used on tugs and ferries.

- Paddle-wheels. In the past, paddle-wheels played a large role in river boats, but have been largely replaced now by propellers or waterjets.